Int. J. Solids Structures, 1970, Vol. 6, pp. 1133 to 1156. Pergamon Press. Printed in Great Britain

A SHALLOW SHELL FINITE ELEMENT OF TRIANGULAR SHAPE

G. R. COWPER,† G. M. LINDBERG† and M. D. OLSON†

National Aeronautical Establishment, Ottawa, Canada

Abstract—A conforming shallow shell finite element of arbitrary triangular shape is developed and applied to the solution of several static problems. The element incorporates 36 generalized coordinates, namely the normal displacement w and its first and second derivatives plus the tangential displacements u and v and their first derivatives at each vertex. The theoretical asymptotic rate of convergence of strain energy when using this element is n^{-6}, where n is the number of elements per side of a structure. The example applications presented demonstrate that accurate predictions of stresses as well as displacements are obtained with only a few elements.

1. INTRODUCTION

CONSIDERABLE progress has been made in the past few years in applying the finite element method to the analysis of shell structures. The initial work in this area was devoted to shells of revolution in which closed rings or conical shell segments were used to model complete structures. Much of this work is reviewed by Jones and Strome [1].

Attempts to develop a finite element method for general shell structures have generally followed two different courses. In the first approach, the shell is replaced by an assemblage of flat plate elements which are either triangular or quadrilateral in shape. Each plate element is connected in some fashion to those surrounding it and undergoes both bending and stretching deformations. This approach has been successfully employed for cylindrical geometry by Hrennikoff and Tezcan [2] and for general shell shapes by Zienkiewicz and Cheung [3], Clough and Johnson [4] and Carr [5]. However, the method has the disadvantage that there is no coupling between bending and stretching within each element, and consequently a large number of elements must be used to achieve satisfactory accuracy.

The second approach, which ultimately should yield better results, is to develop curved shell elements that permit closer geometrical representations of a shell structure. Such an approach has been followed with good results for the case of cylindrical shells where rectangular elements are completely adequate. Successful cylindrical shell elements have been developed by Bogner *et al.* [6], Cantin and Clough [7] and Olson and Lindberg [8].

On the other hand, attempts to develop rectangular or quadrilateral elements for general shells have been only partially successful. For example, Connor and Brebbia [9] have introduced a rectangular element based on shallow shell theory, and Gallagher [10] has developed a quadrilateral element for translational shells. However, both elements use only linear distributions for the tangential displacements and consequently do not incorporate all the required rigid body modes. Although this does not preclude convergence to the correct answer, it does mean that the elements are far too stiff and therefore are quite inefficient.

† Research Officers, Structures and Materials Laboratory.

Several general curved shell elements of arbitrary triangular shape have now been developed. Utku and Melosh [11] have introduced a shallow curved triangular element based only on linear displacement distributions. This element is consequently too stiff. More recently, Strickland and Loden [12] have presented another shallow curved triangular element based on a cubic variation for the normal displacement and linear variations for the tangential displacements. This element is a distinct advancement over the former one but appears to offer little improvement in accuracy over the comparable flat plate model of Clough and Johnson [4]. Bonnes *et al.* [13] have introduced a shallow curved triangular element based on a cubic variation for all three displacement components. They actually present results for two versions of this element, one with 27 degrees of freedom and the other with 36. The latter version incorporates the normal derivatives of u, v and w at mid edge nodes as the extra degrees of freedom and hence allows the normal derivatives to vary quadratically along an edge whereas the former one has only a linear variation. Both elements appear to give somewhat better results than the element of Strickland and Loden [12]. However, the 36 degree of freedom version has the distinct disadvantage of having mid-edge nodes, and the other model is somewhat limited by having only a linear variation of normal directives along each edge.

All the foregoing elements have disadvantages common to triangular plate bending elements as well, and it is not surprising that the development of a good triangular curved shell element has been impeded by the lack of a satisfactory conforming triangular plate bending element. Only recently has such a plate bending element been developed by Cowper *et al.* [14–16] and also by Bell [17, 18] and Butlin and Ford [19]. This element uses as generalized coordinates the transverse displacement and its first and second derivatives at each vertex, a total of 18 in all. The displacement function for the element contains a complete quartic polynomial plus some higher degree terms and allows a cubic variation of the normal slope along each edge. It is shown [15, 16] that use of this element leads to strain energy convergence rates approaching n^{-6}, where n is the number of elements per side of a plate. Along with this rapid rate of convergence, it was also found that remarkably accurate displacement and stress predictions were obtained even with coarse grids of elements.

As a first step in extending this highly successful approach to shells, this paper investigates the application to shallow shells. The shallow shell approximation leads to the significant simplification that all necessary mathematical manipulations may be carried out in the base reference plane. Furthermore, with this approximation, it is sufficient to assume constant geometric curvature over the element.

The displacement function for the normal deflection, w, of the shell is formulated exactly as it was for the plate. That is, w is taken as a quintic polynomial (21 terms) in the two cartesian coordinates in the base plane. Three constraints are placed on the polynomial to ensure that the normal derivative varies cubically along each edge. The tangential displacements u and v for the shell are each expressed as cubic polynomials (10 terms each), and the generalized coordinates are taken to be u and v and their first derivatives at each element vertex, plus u and v at the centroid. However, these two centroidal displacements are condensed out of the final stiffness and load matrices for the element by minimizing the potential energy with respect to them. (This particular representation of the membrane state is the same as that originally suggested by Felippa [20] and extensively studied by Carr [5] for a refined plane stress element.) Hence, the final element has 36 degrees of

freedom and is completely conforming for smooth shells.† Furthermore, it may easily be shown that the element contains an exact representation of three inextensional modes as well as all six required rigid body modes, and has an asymptotic strain energy convergence rate of n^{-6} in complete analogy to the plate bending element.

The derivation of the basic stiffness and consistent load matrices for the element follows the now standard direct stiffness method of calculating potential energy. However, a major advance is achieved in that the matrix components are obtained in closed form relative to the polynomial coefficients. These results are then easily transformed to corner displacement notation in local or global coordinates by simple matrix multiplication.

The resulting element is systematically tested on three problems for which exact solutions are known. The first example application considered is the plane stress problem of a flat square plate loaded on two opposite edges by a parabolically distributed normal stress. This example serves to completely verify how well the shell element works in the limiting case of zero curvatures. The next application considered is that of a shallow spherical cap supported on a square base and subjected to uniform pressure loading. Calculations are carried out for two values of the shell rise parameter corresponding to two different shell boundary layer widths (the boundary layer is sometimes referred to as the edge effect). The results clearly illustrate the effect of the boundary layer on the finite element representations. The final example is the cylindrical shell roof problem used by many authors [4, 5, 7, 12, 13] to test their elements. This example serves to illustrate the superiority of the present element over previous developments.

2. THEORETICAL FORMULATION

2.1 *Strain energy*

The geometry for an arbitrary triangular shallow shell element is shown in Fig. 1. The shell shape is defined by the height $\zeta(\xi, \eta)$ above the base plane, in which ξ, η are taken as local coordinates and x, y as global coordinates. The dimensions a, b, c of the base triangle $1'2'3'$ and the rotation angle θ are easily derived in terms of the global coordinates of the vertices [15].

Following the shallow shell theory of Novozhilov [21], the membrane strains in the shell are given by

$$\begin{aligned} \varepsilon_{\xi\xi} &= u_\xi - \zeta_{\xi\xi} w \\ \varepsilon_{\eta\eta} &= v_\eta - \zeta_{\eta\eta} w \\ \varepsilon_{\xi\eta} &= u_\eta + v_\xi - 2\zeta_{\xi\eta} w \end{aligned} \tag{1}$$

where u and v are the tangential displacements measured parallel to the ξ and η directions, respectively, and w is the normal displacement (Fig. 1). The subscripts on u, v, w and ζ denote differentiation, i.e. $u_\xi = \partial u/\partial\xi$ etc. The bending strains are given by

$$\kappa_{\xi\xi} = -w_{\xi\xi}, \qquad \kappa_{\eta\eta} = -w_{\eta\eta}, \qquad \kappa_{\xi\eta} = -2w_{\xi\eta}. \tag{2}$$

† See Appendix for a rigorous discussion of this point.

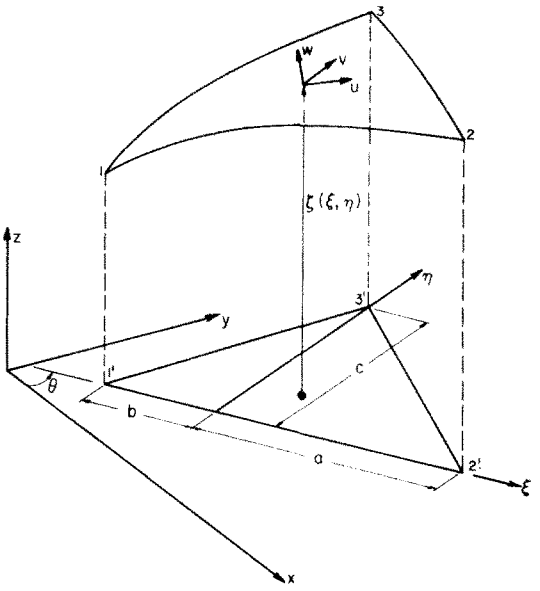

FIG. 1. Shell element geometry and coordinate systems.

Combining the contributions from the membrane and bending strains yields the strain energy density

$$\frac{dU}{dA} = \frac{Et}{2(1-\nu^2)}\{[\varepsilon_{\xi\xi}^2 + \varepsilon_{\eta\eta}^2 + 2\nu\varepsilon_{\xi\xi}\varepsilon_{\eta\eta} + \tfrac{1}{2}(1-\nu)\varepsilon_{\xi\eta}^2] + \frac{t^2}{12}[\kappa_{\xi\xi}^2 + \kappa_{\eta\eta}^2 + 2\nu\kappa_{\xi\xi}\kappa_{\eta\eta} + \tfrac{1}{2}(1-\nu)\kappa_{\xi\eta}^2]\}. \tag{3}$$

For shallow shells, the area of the shell surface is approximately equal to its projected area, and hence equation (3) may be integrated over the base plane. Then combining equations (1)–(3) yields the final strain energy expression

$$\begin{aligned} U = \frac{Et}{2(1-\nu^2)} \iint \Big\{ & [u_\xi^2 + v_\eta^2 + 2\nu u_\xi v_\eta + \tfrac{1}{2}(1-\nu)(u_\eta + v_\xi)^2] \\ & - 2[(\zeta_{\xi\xi} + \nu\zeta_{\eta\eta})u_\xi + (\zeta_{\eta\eta} + \nu\zeta_{\xi\xi})v_\eta + (1-\nu)\zeta_{\xi\eta}(u_\eta + v_\xi)]w \\ & + [\zeta_{\xi\xi}^2 + \zeta_{\eta\eta}^2 + 2\nu\zeta_{\xi\xi}\zeta_{\eta\eta} + 2(1-\nu)\zeta_{\xi\eta}^2]w^2 \\ & + \frac{t^2}{12}[w_{\xi\xi}^2 + w_{\eta\eta}^2 + 2\nu w_{\xi\xi}w_{\eta\eta} + 2(1-\nu)w_{\xi\eta}^2] \Big\} \, d\xi \, d\eta \end{aligned} \tag{4}$$

where the integration is over the base triangle 1′2′3′ in Fig. 1.

In the present work, the function $\zeta(\xi, \eta)$ is assumed to be of quadratic form

$$\zeta(\xi, \eta) = c_1 + c_2\xi + c_3\eta + c_4\xi^2 + c_5\xi\eta + c_6\eta^2. \tag{5}$$

This implies that the shell element has constant curvatures, and this is consistent with the approximations of shallow shell theory. It may be noted from equation (4) that the shell curvatures are the only shape quantities required in calculating strain energy. Therefore, they may be specified for an element directly (which is the approach followed in the present work), or they may be calculated from equation (5) once the constants therein have been determined. One convenient way to do this is to specify the height of the shell at points 1′, 2′ and 3′ and also at the mid-edge points of the element of Fig. 1.

2.2 *Displacements*

As outlined in the Introduction, special displacement functions are required for the present element in order to ensure conformity and high accuracy. The displacement function developed for the conforming plate bending element [15, 16] is used here for the normal displacement w. This function contains a complete quartic polynomial and leads to strain energy convergence rates approaching n^{-6}, where n is the number of elements per side of a plate.

The choice of functions for the tangential displacement components u and v is motivated by the need for an accuracy comparable to that for the normal displacement w. This means that the membrane state representation should also lead to strain energy convergence rates of n^{-6}. To achieve this, it is sufficient to express u and v each as complete cubic polynomials, as may be easily shown by an argument similar to that used in the convergence proof for the plate bending element [15]. That is, complete cubic polynomials can represent the exact displacements u and v with an error of order h^4 within each element, where h is a characteristic linear dimension of the element. The first derivatives of u and v, which are the quantities that enter equation (4), will be represented to order h^3. Hence, since these quantities enter that equation quadratically, the strain energy will be correct to order h^6, provided u and v are continuous between adjacent elements.

Finally, considering that h is inversely proportional to n, the number of elements used per side of a structure, leads to the conclusion that this representation of the membrane state will also lead to strain energy convergence proportional to n^{-6}.

Hence, the starting point for the present shallow shell element is to assume u, v and w in the form (Fig. 1)

$$u = a_1 + a_2\xi + a_3\eta + a_4\xi^2 + a_5\xi\eta + a_6\eta^2 + a_7\xi^3 + a_8\xi^2\eta + a_9\xi\eta^2 + a_{10}\eta^3 \tag{6a}$$

$$v = a_{11} + a_{12}\xi + a_{13}\eta + a_{14}\xi^2 + a_{15}\xi\eta + a_{16}\eta^2 + a_{17}\xi^3 + a_{18}\xi^2\eta + a_{19}\xi\eta^2 + a_{20}\eta^3 \tag{6b}$$

$$\begin{aligned} w = {} & a_{21} + a_{22}\xi + a_{23}\eta + a_{24}\xi^2 + a_{25}\xi\eta + a_{26}\eta^2 + a_{27}\xi^3 + a_{28}\xi^2\eta \\ & + a_{29}\xi\eta^2 + a_{30}\eta^3 + a_{31}\xi^4 + a_{32}\xi^3\eta + a_{33}\xi^2\eta^2 + a_{34}\xi\eta^3 \\ & + a_{35}\eta^4 + a_{36}\xi^5 + a_{37}\xi^3\eta^2 + a_{38}\xi^2\eta^3 + a_{39}\xi\eta^4 + a_{40}\eta^5. \end{aligned} \tag{6c}$$

Note that the expression for w, equation (6c), does not contain the term $\xi^4\eta$, and therefore automatically satisfies the requirement that the normal slope be only cubic along the element edge 1–2. The conditions that ensure only cubic variations of normal slopes along edges 2–3 and 3–1 are the same as for the flat plate case [15, 16] and are

$$5b^4ca_{36} + (3b^2c^3 - 2b^4c)a_{37} + (2bc^4 - 3b^3c^2)a_{38} + (c^5 - 4b^2c^3)a_{39} - 5bc^4a_{40} = 0 \tag{7a}$$

$$5a^4ca_{36} + (3a^2c^3 - 2a^4c)a_{37} - (2ac^4 - 3a^3c^2)a_{38} + (c^5 - 4a^2c^3)a_{39} + 5ac^4a_{40} = 0. \tag{7b}$$

These constraints are just sufficient to reduce the twenty independent parameters of equation (6c) to only eighteen. The generalized displacements for w are then taken to be w and its first and second derivatives at each corner of the element, a total of eighteen which is consistent with the eighteen free parameters available. The generalized displacements for u and v are taken to be u and v and their first derivatives at each corner plus u and v at the element's centroid. This gives a total of twenty which is consistent with the twenty free parameters of equations (6a) and (6b). All the generalized displacements are assembled into a 38 column vector $\{W_1\}$, first in the local coordinate system ξ, η.

$$\{W_1\}^T = (u_1, u_{\xi 1}, u_{\eta 1}, v_1, v_{\xi 1}, v_{\eta 1}, w_1, w_{\xi 1}, w_{\eta 1},$$

$$w_{\xi\xi 1}, w_{\xi\eta 1}, w_{\eta\eta 1}, u_2, \ldots, u_3, \ldots, u_c, v_c) \tag{8}$$

where $u_\xi = \partial u/\partial \xi$, etc. The subscripts 1, 2, 3, c denote the corners 1, 2 and 3 and the centroid of the element, respectively. The coefficients a_i of equations (6) are assembled into a 40 column vector $\{A\}$ where

$$\{A\}^T = (a_1, a_2, \ldots, a_{40}) \tag{9}$$

and combining equations (6)–(9) yields the matrix relation

$$\begin{Bmatrix} W_1 \\ 0 \\ 0 \end{Bmatrix} = [T]\{A\} \tag{10}$$

where the 40×40 transformation matrix $[T]$ is given in Table 1.

The determinant of $[T]$ has the value $-64c^{34}(a+b)^{31}(a^2+c^2)(b^2+c^2)/729$, which is nonzero for all practical problems. Hence, equation (10) may be inverted to give

$$\{A\} = [T^{-1}]\begin{Bmatrix} W_1 \\ 0 \\ 0 \end{Bmatrix} = [T_1]\{W_1\} \tag{11}$$

where the 40×38 matrix $[T_1]$ consists of the first 38 columns of $[T^{-1}]$.

2.3 *Stiffness matrix*

The stiffness matrix for the element is obtained from a calculation of strain energy. The displacement functions of equations (6) are substituted in equation (4) and the integration carried out to yield the quadratic strain energy form

$$U = \frac{Et}{2(1-\nu^2)}\{A\}^T[k]\{A\}. \tag{12}$$

The entries of the stiffness matrix $[k]$ may be determined in closed form just as they were for the plate bending element [15, 16].

TABLE 1. TRANSFORMATION MATRIX [T]

$$[T] = \begin{bmatrix} S_1 & 0 & 0 \\ 0 & S_1 & 0 \\ 0 & 0 & S_2 \\ S_3 & 0 & 0 \\ 0 & S_3 & 0 \\ 0 & 0 & S_4 \\ S_5 & 0 & 0 \\ 0 & S_5 & 0 \\ 0 & 0 & S_6 \\ S_7 & 0 & 0 \\ 0 & S_7 & 0 \\ 0 & 0 & S_8 \end{bmatrix}$$

$$[S_1] = \begin{bmatrix} 1 & -b & 0 & b^2 & 0 & 0 & -b^3 & 0 & 0 & 0 \\ 0 & 1 & 0 & -2b & 0 & 0 & 3b^2 & 0 & 0 & 0 \\ 0 & 0 & 1 & 0 & -b & 0 & 0 & b^2 & 0 & 0 \end{bmatrix}$$

$$[S_2] = \begin{bmatrix} 1 & -b & 0 & b^2 & 0 & 0 & -b^3 & 0 & 0 & 0 & b^4 & 0 & 0 & 0 & 0 & -b^5 & 0 & 0 & 0 & 0 \\ 0 & 1 & 0 & -2b & 0 & 0 & 3b^2 & 0 & 0 & 0 & -4b^3 & 0 & 0 & 0 & 0 & 5b^4 & 0 & 0 & 0 & 0 \\ 0 & 0 & 1 & 0 & -b & 0 & 0 & b^2 & 0 & 0 & 0 & -b^3 & 0 & 0 & 0 & 0 & 0 & 0 & 0 & 0 \\ 0 & 0 & 0 & 2 & 0 & 0 & -6b & 0 & 0 & 0 & 12b^2 & 0 & 0 & 0 & 0 & -20b^3 & 0 & 0 & 0 & 0 \\ 0 & 0 & 0 & 0 & 1 & 0 & 0 & -2b & 0 & 0 & 0 & 3b^2 & 0 & 0 & 0 & 0 & 0 & 0 & 0 & 0 \\ 0 & 0 & 0 & 0 & 0 & 2 & 0 & 0 & -2b & 0 & 0 & 0 & 2b^2 & 0 & 0 & 0 & -2b^3 & 0 & 0 & 0 \end{bmatrix}$$

$$[S_3] = \begin{bmatrix} 1 & a & 0 & a^2 & 0 & 0 & a^3 & 0 & 0 & 0 \\ 0 & 1 & 0 & 2a & 0 & 0 & 3a^2 & 0 & 0 & 0 \\ 0 & 0 & 1 & 0 & a & 0 & 0 & a^2 & 0 & 0 \end{bmatrix}$$

$$[S_4] = \begin{bmatrix} 1 & a & 0 & a^2 & 0 & 0 & a^3 & 0 & 0 & 0 & a^4 & 0 & 0 & 0 & 0 & a^5 & 0 & 0 & 0 & 0 \\ 0 & 1 & 0 & 2a & 0 & 0 & 3a^2 & 0 & 0 & 0 & 4a^3 & 0 & 0 & 0 & 0 & 5a^4 & 0 & 0 & 0 & 0 \\ 0 & 0 & 1 & 0 & a & 0 & 0 & a^2 & 0 & 0 & 0 & a^3 & 0 & 0 & 0 & 0 & 0 & 0 & 0 & 0 \\ 0 & 0 & 0 & 2 & 0 & 0 & 6a & 0 & 0 & 0 & 12a^2 & 0 & 0 & 0 & 0 & 20a^3 & 0 & 0 & 0 & 0 \\ 0 & 0 & 0 & 0 & 1 & 0 & 0 & 2a & 0 & 0 & 0 & 3a^2 & 0 & 0 & 0 & 0 & 0 & 0 & 0 & 0 \\ 0 & 0 & 0 & 0 & 0 & 2 & 0 & 0 & 2a & 0 & 0 & 0 & 2a^2 & 0 & 0 & 0 & 2a^3 & 0 & 0 & 0 \end{bmatrix}$$

$$[S_5] = \begin{bmatrix} 1 & 0 & c & 0 & 0 & c^2 & 0 & 0 & 0 & c^3 \\ 0 & 1 & 0 & 0 & c & 0 & 0 & 0 & c^2 & 0 \\ 0 & 0 & 1 & 0 & 0 & 2c & 0 & 0 & 0 & 3c^2 \end{bmatrix}$$

$$[S_6] = \begin{bmatrix} 1 & 0 & c & 0 & 0 & c^2 & 0 & 0 & 0 & c^3 & 0 & 0 & 0 & 0 & c^4 & 0 & 0 & 0 & 0 & c^5 \\ 0 & 1 & 0 & 0 & c & 0 & 0 & 0 & c^2 & 0 & 0 & 0 & 0 & c^3 & 0 & 0 & 0 & 0 & c^4 & 0 \\ 0 & 0 & 1 & 0 & 0 & 2c & 0 & 0 & 0 & 3c^2 & 0 & 0 & 0 & 0 & 4c^3 & 0 & 0 & 0 & 0 & 5c^4 \\ 0 & 0 & 0 & 2 & 0 & 0 & 0 & 2c & 0 & 0 & 0 & 0 & 2c^2 & 0 & 0 & 0 & 0 & 2c^3 & 0 & 0 \\ 0 & 0 & 0 & 0 & 1 & 0 & 0 & 0 & 2c & 0 & 0 & 0 & 0 & 3c^2 & 0 & 0 & 0 & 0 & 4c^3 & 0 \\ 0 & 0 & 0 & 0 & 0 & 2 & 0 & 0 & 0 & 6c & 0 & 0 & 0 & 0 & 12c^2 & 0 & 0 & 0 & 0 & 20c^3 \end{bmatrix}$$

$$[S_7] = \begin{bmatrix} 1 & \frac{a-b}{3} & \frac{c}{3} & \frac{(a-b)^2}{9} & \frac{(a-b)c}{9} & \frac{c^2}{9} & \frac{(a-b)^3}{27} & \frac{(a-b)^2 c}{27} & \frac{(a-b)c^2}{27} & \frac{c^3}{27} \end{bmatrix}$$

$$[S_8] = \begin{bmatrix} 0 & 0 & 0 & 0 & 0 & 0 & 0 & 0 & 0 & 0 & 0 & 0 & 0 & 0 & 0 & 5a^4c, & 3a^2c^3-2a^4c, & -2ac^4+3a^3c^2, & c^5-4a^2c^3, & 5ac^4 \\ 0 & 0 & 0 & 0 & 0 & 0 & 0 & 0 & 0 & 0 & 0 & 0 & 0 & 0 & 0 & 5b^4c, & 3b^2c^3-2b^4c, & 2bc^4-3b^3c^2, & c^5-4b^2c^3, & -5bc^4 \end{bmatrix}$$

This may be carried out most easily by rewriting equations (6) as

$$u = \sum_{i=1}^{10} a_i \xi^{m_i} \eta^{n_i} \tag{13a}$$

$$v = \sum_{i=11}^{20} a_i \xi^{p_i} \eta^{q_i} \tag{13b}$$

$$w = \sum_{i=21}^{40} a_i \xi^{r_i} \eta^{s_i}. \tag{13c}$$

Then substituting equations (13) into equation (4) and incorporating the symmetry requirement yields

$$\begin{aligned}k_{ij} = {} & m_i m_j F(m_i+m_j-2, n_i+n_j)+q_i q_j F(p_i+p_j, q_i+q_j-2)+\tfrac{1}{2}(1-\nu)[n_i n_j F(m_i+m_j, n_i+n_j-2)\\ & + p_i p_j F(p_i+p_j-2, q_i+q_j)]+[\tfrac{1}{2}(1-\nu)n_j p_i+\nu m_j q_i]F(m_j+p_i-1, n_j+q_i-1)\\ & + [\tfrac{1}{2}(1-\nu)n_i p_j+\nu m_i q_j]F(m_i+p_j-1, n_i+q_j-1)-(\zeta_{\xi\xi}+\nu\zeta_{\eta\eta})[m_i F(m_i+r_j-1, n_i+s_j)\\ & + m_j F(m_j+r_i-1, n_j-s_i)]-(\zeta_{\eta\eta}+\nu\zeta_{\xi\xi})[q_i F(p_i+r_j, q_i+s_j-1)+q_j F(p_j+r_i, q_j+s_i-1)]\\ & -(1-\nu)\zeta_{\xi\eta}[n_i F(m_i+r_j, n_i+s_j-1)+n_j F(m_j+r_i, n_j+s_i-1)+p_i F(p_i+r_j-1, q_i+s_j)\\ & + p_j F(p_j+r_i-1, q_j+s_i)]+[\zeta_{\xi\xi}^2+\zeta_{\eta\eta}^2+2\nu\zeta_{\xi\xi}\zeta_{\eta\eta}+2(1-\nu)\zeta_{\xi\eta}^2]F(r_i+r_j, s_i+s_j)\\ & +(t^2/12)\{r_i r_j(r_i-1)(r_j-1)F(r_i+r_j-4, s_i+s_j)+s_i s_j(s_i-1)(s_j-1)F(r_i+r_j, s_i+s_j-4)\\ & + [2(1-\nu)r_i r_j s_i s_j+\nu r_i s_j(r_i-1)(s_j-1)+\nu r_j s_i(r_j-1)(s_i-1)]F(r_i+r_j-2, s_i+s_j-2)\} \quad (14)\end{aligned}$$

where

$$F(m, n) = c^{n+1}[a^{m+1}-(-b)^{m+1}]\frac{m!n!}{(m+n+2)!}. \quad (15)$$

Note that i and j run from 1 to 40, and therefore m_i and n_i are defined to be zero for $i > 10$, p_i and q_i are zero for $i < 11$ and $i > 20$, and r_i and s_i are zero for $i < 21$. All the computations involved in evaluating the k_{ij} from equation (14) are carried out within the computer once the values of a, b, c, m_i, n_i, p_i, q_i, r_i and s_i are furnished.

Combining equations (11) and (12) yields the strain energy in terms of $\{W_1\}$ as

$$U = \frac{Et}{2(1-\nu^2)}\{W_1\}^T[K_1]\{W_1\} \quad (16)$$

where

$$[K_1] = [T_1]^T[k][T_1] \quad (17)$$

is the 38×38 stiffness matrix in terms of the generalized displacements relative to the local coordinate system ξ, η. This matrix is now transformed to the global coordinate system x, y using

$$\{W_1\} = [R]\{W_2\} \quad (18)$$

where

$$\{W_2\}^T = (u_1, u_{x1}, u_{y1}, v_1, v_{x1}, v_{y1}, w_1, w_{x1}, w_{y1}, w_{xx1}, w_{xy1}, w_{yy1}, u_2, \ldots, u_3, \ldots, u_c\, v_c) \quad (19)$$

is the generalized displacement vector relative to global coordinates, and $[R]$ is the rotation matrix given in Table 2. Then combining equations (16), (17) and (18) yields

$$U = \frac{Et}{2(1-\nu^2)}\{W_2\}^T[K_2]\{W_2\} \quad (20)$$

where

$$[K_2] = [R]^T[T_1]^T[k][T_1][R] \quad (21)$$

is the 38×38 stiffness matrix relative to global coordinates.

TABLE 2. ROTATION MATRIX [R]

$$R = \begin{bmatrix} R_1 & 0 & 0 & 0 & 0 & 0 & 0 \\ 0 & R_2 & 0 & 0 & 0 & 0 & 0 \\ 0 & 0 & R_1 & 0 & 0 & 0 & 0 \\ 0 & 0 & 0 & R_2 & 0 & 0 & 0 \\ 0 & 0 & 0 & 0 & R_1 & 0 & 0 \\ 0 & 0 & 0 & 0 & 0 & R_2 & 0 \\ 0 & 0 & 0 & 0 & 0 & 0 & R_3 \end{bmatrix}$$

where

$$[R_1] = \begin{bmatrix} \cos\theta & 0 & 0 & \sin\theta & 0 & 0 \\ 0 & \cos^2\theta & \sin\theta\cos\theta & 0 & \sin\theta\cos\theta & \sin^2\theta \\ 0 & -\sin\theta\cos\theta & \cos^2\theta & 0 & -\sin^2\theta & \sin\theta\cos\theta \\ -\sin\theta & 0 & 0 & \cos\theta & 0 & 0 \\ 0 & -\sin\theta\cos\theta & -\sin^2\theta & 0 & \cos^2\theta & \sin\theta\cos\theta \\ 0 & \sin^2\theta & -\sin\theta\cos\theta & 0 & -\sin\theta\cos\theta & \cos^2\theta \end{bmatrix}$$

$$[R_2] = \begin{bmatrix} 1 & 0 & 0 & 0 & 0 & 0 \\ 0 & \cos\theta & \sin\theta & 0 & 0 & 0 \\ 0 & -\sin\theta & \cos\theta & 0 & 0 & 0 \\ 0 & 0 & 0 & \cos^2\theta & 2\sin\theta\cos\theta & \sin^2\theta \\ 0 & 0 & 0 & -\sin\theta\cos\theta & \cos^2\theta-\sin^2\theta & \sin\theta\cos\theta \\ 0 & 0 & 0 & \sin^2\theta & -2\sin\theta\cos\theta & \cos^2\theta \end{bmatrix}$$

$$[R_3] = \begin{bmatrix} \cos\theta & \sin\theta \\ -\sin\theta & \cos\theta \end{bmatrix}$$

2.4 *Consistent load vector*

The consistent load vector is obtained by calculating the virtual work done by the applied loads $Q_u(\xi, \eta)$, $Q_v(\xi, \eta)$ and $Q_w(\xi, \eta)$ in the u, v and w directions, respectively. The transformed load vector becomes

$$\{P\} = [R]^T[T_1]^T\{Q\} \tag{22}$$

where the entries in the column vector $\{Q\}$ are

$$Q_i = \begin{cases} \int\int Q_u \xi^{m_i}\eta^{n_i}\,d\xi\,d\eta, & i < 11 \\ \int\int Q_v \xi^{p_i}\eta^{q_i}\,d\xi\,d\eta, & 10 < i < 21 \\ \int\int Q_w \xi^{r_i}\eta^{s_i}\,d\xi\,d\eta, & i > 20 \end{cases} \tag{23}$$

where the integration is over the base triangle 1′ 2′ 3′ of Fig. 1. In the special case of a uniform pressure load of intensity Q_0

$$Q_i = \begin{cases} 0 & i < 21 \\ -Q_0 F(r_i, s_i), & i > 20. \end{cases} \tag{24}$$

2.5 *Condensation of stiffness matrix*

Before proceeding to use the element just derived, it is convenient to condense out the centroidal displacements u_c and v_c. It may be noted that these displacements, since they lie inside the element, will be unaffected when the elements are joined together to represent a structure. Hence, they may be eliminated before the elements are joined without affecting the final results. It is advantageous to do this because it will reduce the number of degrees of freedom in each element and will also simplify the process of assembling elements. The reduction is carried out by minimizing the potential energy in one element. The matrix equation of equilibrium for an element is written in the partitioned form

$$[K_2]\{W_2\} = \left[\begin{array}{c|c} K_0 & K_{0c} \\ \hline K_{0c}^T & K_c \end{array}\right] \left\{\begin{array}{c} W \\ \hline W_c \end{array}\right\} = \left\{\begin{array}{c} P_0 \\ \hline P_c \end{array}\right\} \tag{25}$$

where $\{W_c\}$ is the two component vector $(u_c, v_c)^T$ and $\{W\}$ contains the first 36 components of equation (19).

Equation (25) is separated into two equations and $\{W_c\}$ is eliminated to yield

$$[K]\{W\} = \{P\} \tag{26}$$

where

$$[K] = [K_0] - [K_{0c}][K_c^{-1}][K_{0c}]^T \tag{27}$$

is the reduced 36×36 stiffness matrix, and

$$\{P\} = \{P_0\} - [K_{0c}][K_c^{-1}]\{P_c\} \tag{28}$$

is the reduced 36 consistent load vector for the shell element.

3. NUMERICAL APPLICATIONS

3.1 *Flat plate examples*

It is worthwhile to first consider the limiting case of a flat plate. In this case, the bending state and the plane stress or membrane state uncouple and each may be solved independently. The bending element has already been thoroughly tested [15, 16]. It may be noted that strain energy convergence rates approaching n^{-6} were actually achieved in several examples, and excellent accuracy was obtained in all cases.

The plane stress problem illustrated in Fig. 2 is used to check out the plane stress element. The problem is a square plate loaded on two opposite sides by a parabolically distributed normal stress. The other two sides are stress free. Timoshenko [22] has presented an approximate energy solution for this problem, but for comparison with finite element solutions, it is necessary to have a more exact solution. Such a solution was obtained by using trigonometric and hyperbolic series expansions, analogous to Timoshenko's solution for the bending of a clamped rectangular plate [23]. A rigorous error analysis was

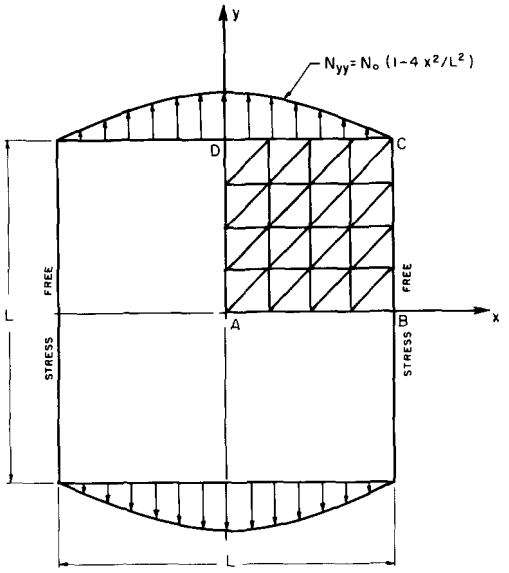

FIG. 2. Parabolically loaded plane stress problem ($n = 8$ shown).

performed to establish limits on truncation errors, so that the accuracy of calculated stresses and displacements could be guaranteed.

The problem is solved with the plane stress elements as indicated in Fig. 2 using various gridworks for the quarter plate. A consistent load vector is obtained to represent the parabolic stress distribution along the edge CD. Some of the numerical results for displacements and stresses at points A, B, C and D as well as strain energy are presented in Table 3,

TABLE 3. NUMERICAL RESULTS FOR PARABOLICALLY LOADED PLANE STRESS PROBLEM

Finite element grids	$\frac{10Etu_B}{(1-\nu^2)N_0L}$	$\frac{10^2Etu_C}{(1-\nu^2)N_0L}$	$\frac{10Etv_C}{(1-\nu^2)N_0L}$	$\frac{10Etv_D}{(1-\nu^2)N_0L}$	$\frac{10N_{xxA}}{N_0}$
1×1	−1·507941	2·1934	1·31824	5·085466	−1·44190
2×2	−1·519812	1·8684	1·28574	5·073595	−1·40137
3×3	−1·519773	1·8046	1·27936	5·073633	−1·40559
4×4	−1·519862	1·7896	1·27787	5·073544	−1·40789
5×5	−1·519900	1·7852	1·27742	5·073507	−1·40880
Exact	−1·519928	1·7837	1·27727	5·073478	−1·40954

$\frac{10N_{yyA}}{N_0}$	$\frac{N_{xxB}}{N_0}$	$\frac{10N_{yyB}}{N_0}$	$\frac{N_{xxC}}{N_0}$	Strain energy $10Et^2U/(1-\nu^2)L^2N_0^2$
8·55810	0·039928	4·70735	0·03181	2·7879813
8·59863	0·004235	4·17500	−0·00005	2·7933662
8·59441	0·000848	4·11902	−0·00299	2·7935404
8·59211	0·000329	4·10971	−0·00285	2·7935617
8·59120	0·000166	4·10767	−0·00233	2·7935667
8·59046	0	4·10670	0	2·7935695

Note: $N_{yyD} = N_{xxB} + N_0$, $N_{xxD} = N_{yyB}$, $N_{yyC} = N_{xxC}$.

and convergence plots of these quantities are given in Fig. 3. Note that no attempt is made to satisfy stress boundary conditions, and hence correct values of stresses on the boundaries are obtained only as $n \to \infty$.

The first result to be noted is that the strain energy convergence rate appears to be slightly less than n^{-5}, which is somewhat lower than the predicted asymptotic rate of n^{-6}. On the other hand, the actual error in strain energy is very small (10^{-6} for $n = 10$) and therefore it is clear that the element gives excellent accuracy.

As seen in Fig. 3, the displacement and stress results seem to convergence quite rapidly. The only odd result is the peculiar kink in the curves for N_{yyC}, N_{xxC}, u_B and v_D for $n = 4$. It may be noted from Table 3 that N_{yyC} and N_{xxC} change sign between $n = 2$ and 4 and, furthermore have extraordinarily small magnitudes for $n = 4$. Hence, the especially small error in u_B and v_D for $n = 4$ must be associated with the fact that N_{yyC} and N_{xxC} are fortuitously close to their exact values for this case. Finally, it may be noted that v_D which is the largest displacement obtained in this problem, is predicted to within 0·001 percent with the $n = 10$ gridwork of the plane stress elements.

3.2 *Spherical cap example*

The shallow shell finite element is now applied to the analysis of the shallow spherical shell shown in Fig. 4. The shell is loaded by a uniform pressure p_0 and is freely supported on a boundary of square planform. Freely supported as used here means that w and u are

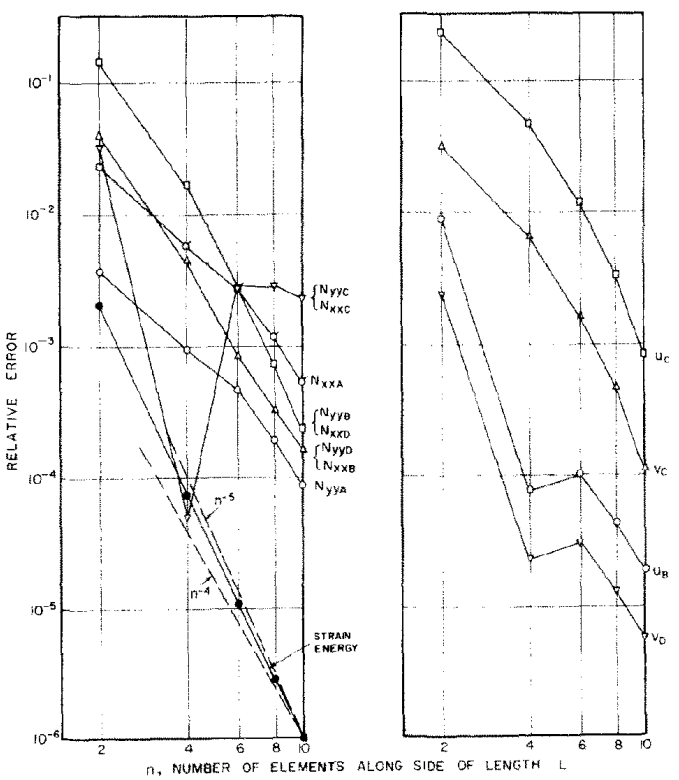

FIG. 3. Relative error in stress, displacement and strain energy predictions for parabolically loaded plane stress problem.

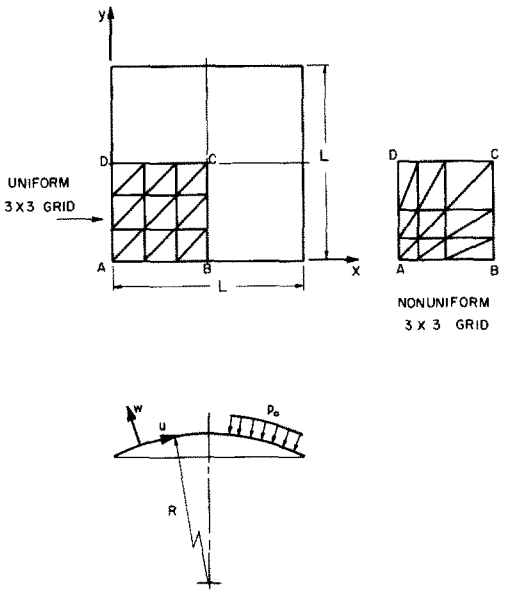

FIG. 4. Spherical cap geometry.

constrained to be zero along the edges $y = 0$ and L, and w and v are zero along $x = 0$ and L. The problem is a good test case, since it has an exact solution in the form of a double sine series [24]. Furthermore, the finite elements can fit the rectangular boundary exactly thus eliminating any error in approximating the boundary shape. This allows a clear evaluation of how well the finite elements approximate the shell behaviour.

The shell is analyzed for two values of the parameter Rt/L^2, namely 0·02 and 0·005. These two values correspond to effective shell boundary layer widths of about $L/6$ and $L/12$, respectively. Using symmetry, only one quarter of the shell is modelled, and the calculations are carried out for uniform gridworks of 1×1, 2×2 and 3×3 arrays with orientations as indicated in Fig. 4. The calculations are also carried out using the non-uniform 3×3 grid shown in the figure for the shell configuration with the smallest boundary layer, $Rt/L^2 = 0{\cdot}005$. The sides AB and AD were subdivided into lengths with ratios 2:3:5 for this case.

Typical numerical results are presented in Tables 4 and 5 for displacements, membrane forces and moments at points A, B and C and also for the total strain energy in the shell. Absolute values of the relative errors in these quantities are plotted in Fig. 5 vs. n, the number of elements along a full edge of the shell, and typical distributions along the lines AB and BC are plotted in Figs. 6–9 as obtained from the uniform element arrays.

The excellent accuracy and rapid convergence of the approximations obtained with the present element are clear from these results. Furthermore, it appears that for most of the quantities listed in Tables 4 and 5 this convergence is monotonic (excluding the non-uniform 3×3 grid results). The main exceptions to this are the quantities M_{xy} and N_{xy} at the corner A, and in fact, the predictions for these quantities exhibit the largest errors. It is interesting that in the comparable flat plate problem [15, 16], the M_{xyA} or corner reaction also exhibited the largest error and slowest convergence rate. It may also be noted that as Rt/L^2 goes to zero, the present shell approaches a membrane and N_{xy} at the corner becomes

TABLE 4. NUMERICAL RESULTS FOR SPHERICAL CAP PROBLEM, $Rt/L^2 = 0{\cdot}02$

Finite element grids	$\frac{Etw_C}{p_0R^2}$	$\frac{10N_{xxC}}{p_0R}$	$\frac{10^3M_{xxC}}{p_0Rt}$	$\frac{10Etv_B}{p_0RL}$	$\frac{N_{xxB}}{p_0R}$
1×1	$-1{\cdot}039564$	$-7{\cdot}951$	$18{\cdot}08$	$-3{\cdot}54786$	$0{\cdot}0284$
2×2	$-1{\cdot}012863$	$-5{\cdot}248$	$-1{\cdot}635$	$-3{\cdot}66585$	$-0{\cdot}0057$
3×3	$-1{\cdot}009819$	$-5{\cdot}111$	$-8{\cdot}873$	$-3{\cdot}67742$	$-0{\cdot}0043$
Exact	$-1{\cdot}009785$	$-5{\cdot}049$	$-8{\cdot}487$	$-3{\cdot}67936$	0

$\frac{N_{yyB}}{p_0R}$	$\frac{M_{xxB}}{p_0Rt}$	$\frac{M_{yyB}}{p_0Rt}$	$\frac{10M_{xyA}}{p_0Rt}$	$\frac{N_{xyA}}{p_0R}$	$\frac{10EtU}{p_0^2L^2R^2}$
$0{\cdot}0947$	$0{\cdot}0088$	$0{\cdot}0293$	$-1{\cdot}095$	$-1{\cdot}371$	$3{\cdot}84025$
$-0{\cdot}0189$	$0{\cdot}0016$	$0{\cdot}0053$	$-1{\cdot}242$	$-1{\cdot}300$	$3{\cdot}89319$
$-0{\cdot}0144$	$0{\cdot}0004$	$0{\cdot}0014$	$-1{\cdot}165$	$-1{\cdot}229$	$3{\cdot}89863$
0	0	0	$-1{\cdot}059$	$-1{\cdot}159$	$3{\cdot}89958$

TABLE 5. NUMERICAL RESULTS FOR SPHERICAL CAP PROBLEM, $Rt/L^2 = 0{\cdot}005$

Finite element grids	$\frac{Etw_C}{p_0R^2}$	$\frac{10N_{xxC}}{p_0R}$	$\frac{10^5M_{xxC}}{p_0Rt}$	$\frac{10Etv_B}{p_0RL}$	$\frac{N_{xxB}}{p_0R}$
1×1	$-1{\cdot}044645$	$-10{\cdot}212$	$1511{\cdot}9$	$-3{\cdot}88215$	$0{\cdot}1267$
2×2	$-0{\cdot}984333$	$-5{\cdot}125$	$-953{\cdot}4$	$-3{\cdot}99105$	$0{\cdot}0295$
3×3	$-1{\cdot}000241$	$-5{\cdot}013$	$-20{\cdot}27$	$-4{\cdot}02524$	$0{\cdot}0029$
3×3*	$-0{\cdot}997084$	$-5{\cdot}015$	$-140{\cdot}0$	$-4{\cdot}03158$	$-0{\cdot}0050$
Exact	$-1{\cdot}000429$	$-5{\cdot}002$	$3{\cdot}1$	$-4{\cdot}03196$	0

$\frac{N_{yyB}}{p_0R}$	$\frac{M_{xxB}}{p_0Rt}$	$\frac{M_{yyB}}{p_0Rt}$	$\frac{10M_{xyA}}{p_0Rt}$	$\frac{N_{xyA}}{p_0R}$	$\frac{10EtU}{p_0^2L^2R^2}$
$0{\cdot}4224$	$0{\cdot}0249$	$0{\cdot}0831$	$-0{\cdot}3588$	$-1{\cdot}4881$	$4{\cdot}20345$
$0{\cdot}0982$	$0{\cdot}0147$	$0{\cdot}0488$	$-0{\cdot}9975$	$-1{\cdot}7564$	$4{\cdot}40870$
$0{\cdot}0098$	$0{\cdot}0048$	$0{\cdot}0161$	$-1{\cdot}2499$	$-1{\cdot}7781$	$4{\cdot}43990$
$-0{\cdot}0166$	$0{\cdot}0011$	$0{\cdot}0038$	$-1{\cdot}2052$	$-1{\cdot}6904$	$4{\cdot}44846$
0	0	0	$-1{\cdot}0582$	$-1{\cdot}6001$	$4{\cdot}44990$

* Nonuniform array (see Fig. 4).

logarithmically singular. Hence, it appears clear that predicting M_{xy} and N_{xy} in the corner A provides the severest test of the finite element approximation.

Again, since no attempt is made to satisfy stress boundary conditions, the moments M_{xx} and M_{yy} and the forces N_{xx} and N_{yy} are not zero at B. However, it is clear from Tables 4 and 5 that these quantities do converge rapidly to zero as the finite element modelling is systematically refined.

While the actual strain energy convergence is strictly monotonic as predicted, its rate of change with n is far from the asymptotic rate of n^{-6}. For instance, the strain energy error slope between $n = 4$ and 6 is approximately $-4{\cdot}7$ and $-3{\cdot}5$ for $Rt/L^2 = 0{\cdot}02$ and $0{\cdot}005$,

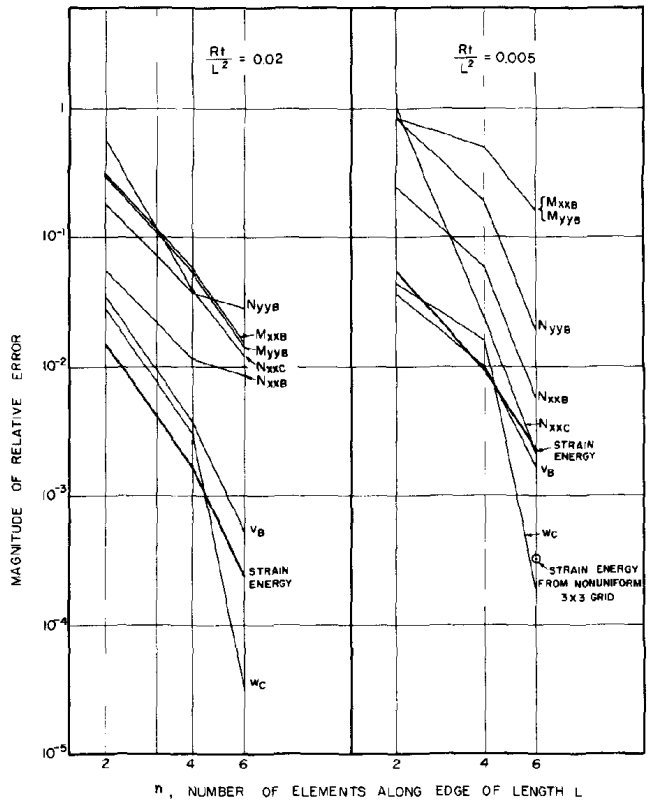

FIG. 5. Relative error of finite element solutions for spherical cap problem.

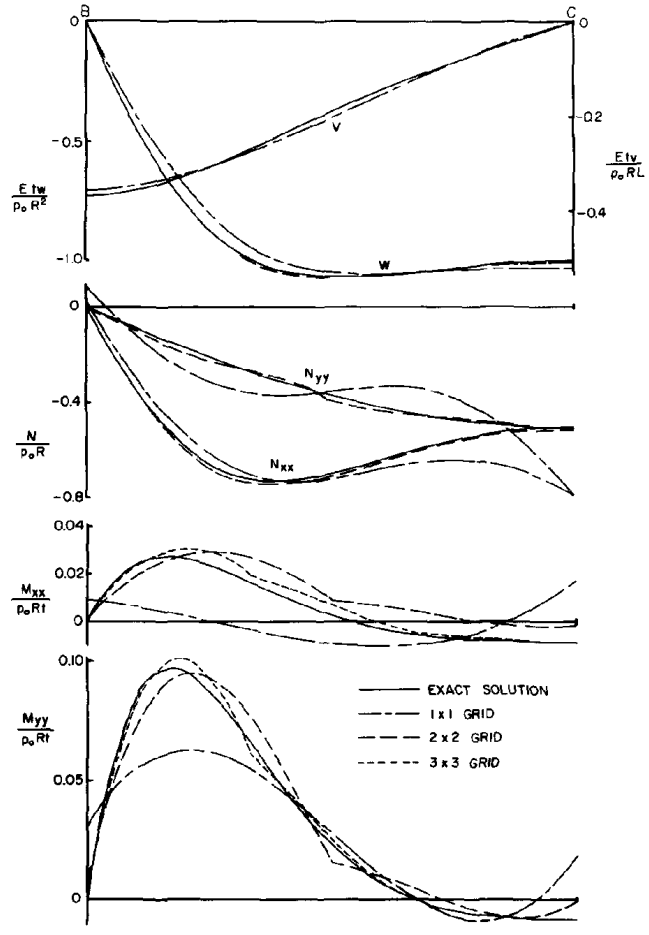

FIG. 6. Distributions along BC in spherical cap problem, $Rt/L^2 = 0{\cdot}02$.

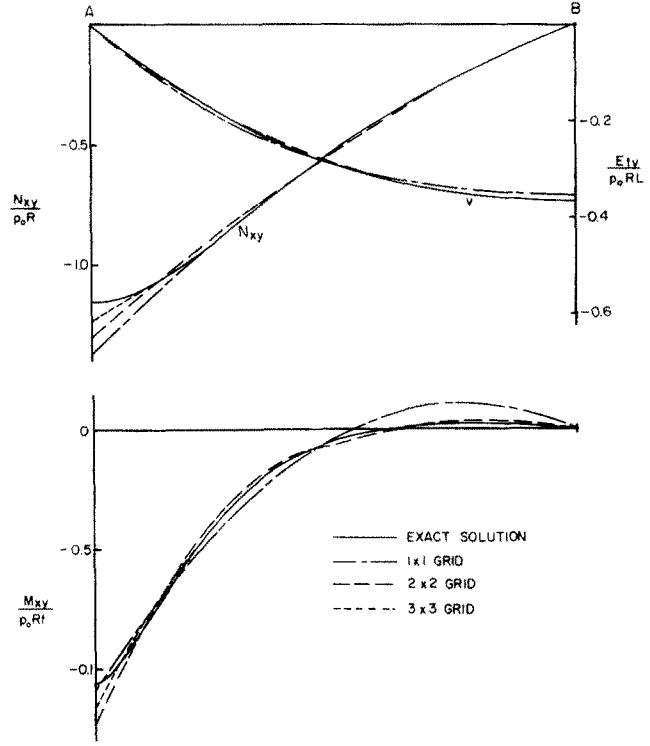

FIG. 7. Distributions along AB in spherical cap problem, $Rt/L^2 = 0{\cdot}02$.

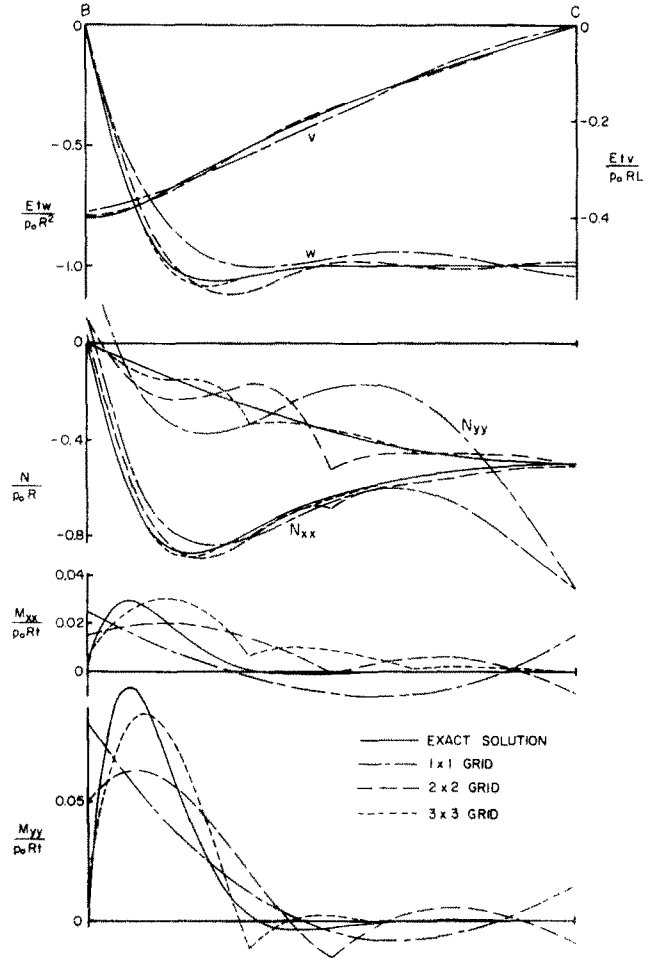

FIG. 8. Distributions along BC in spherical cap problem, $Rt/L^2 = 0{\cdot}005$.

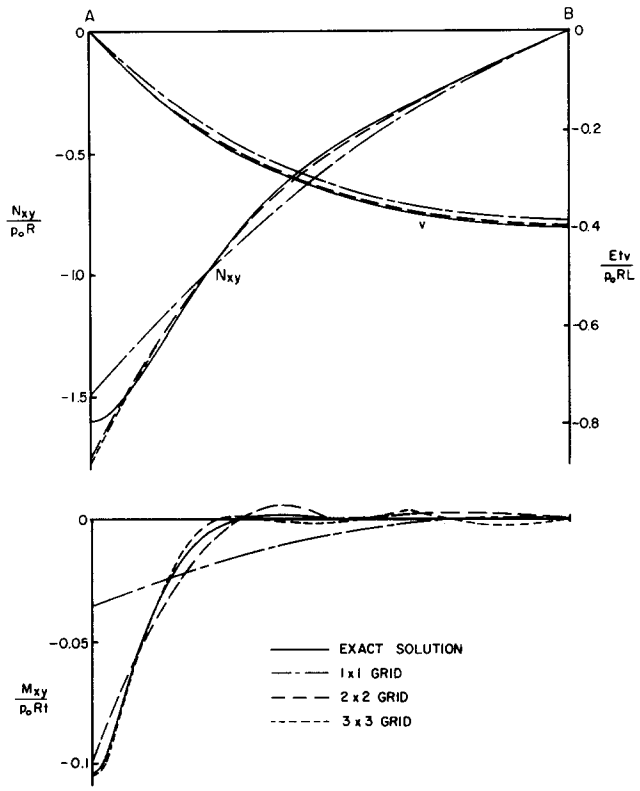

FIG. 9. Distributions along AB in spherical cap problem, $Rt/L^2 = 0{\cdot}005$.

respectively. It appears that the reduction of the boundary layer width associated with the decrease in Rt/L^2 is quite detrimental to this convergence rate. Hence, it appears that the finite element sizes would have to be reduced well below the boundary layer width before the asymptotic rate of convergence could ever be attained. Finally, it may be noted from Fig. 5 that rearranging the elements in the 3×3 grid to the nonuniform case shown in Fig. 4 reduces the error in strain energy by about one order of magnitude.

The distributions plotted in Figs. 6–9 reveal many interesting features of the present finite element method. Firstly, as expected, the displacements are predicted very accurately, the membrane forces somewhat less accurately and of course bending moments less accurately still. However, these bending moment predictions are still remarkably good considering that the finest element gridwork employed is only 3×3 with only 120 degrees of freedom after boundary conditions. It is interesting to note how the finite element predictions oscillate about the exact curves sometimes yielding, for the coarser grids, quite large discrepancies at points A, B and C. It is seen that although the membrane forces and bending moments are continuous at element nodes, they do exhibit kinks there. However, these kinks tend to disappear as the finite element grids are progressively refined.

The reduction of the boundary layer width associated with the reduction of Rt/L^2 from 0·02 to 0·005 has the effect of increasing the error in the predictions, especially near the boundaries. This fact is also shown quite clearly in Fig. 5. This increase in error is easily attributable to the steeper gradients encountered near the boundaries, and an obvious way

to counteract these effects is to reduce the finite element sizes in that region. When this is done using an irregular grid (Fig. 4), the results of Fig. 10 are obtained (see also the numerical results in Table 5). It is seen that a substantial increase in accuracy for membrane forces and bending moments is obtained, especially near the boundaries.

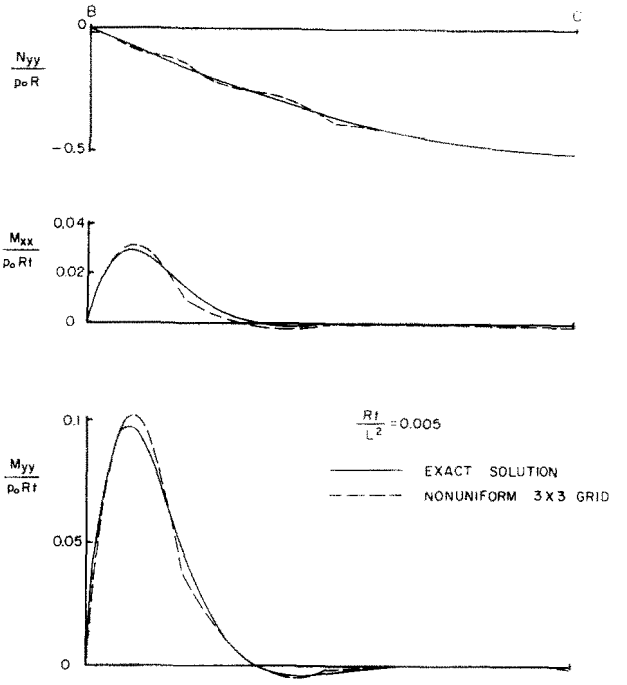

FIG. 10. Membrane force and moment distributions along *BC* for spherical cap problem using nonuniform finite element array.

3.3 *Cylindrical shell roof problem*

The final example application is the cylindrical shell roof problem shown in Fig. 11. The shell is loaded by its own dead weight and is supported by diaphragms at the ends but is free along the sides. Using symmetry, only one quarter of the shell is analyzed, and various uniform gridworks of elements are used with orientations as shown. The numerical data given in the figure are used in the calculations, so that the results may be compared directly with those of other authors.

Most of these authors have compared their results with the so-called exact calculations of Scordelis and Lo [25], which in turn are based on the theory of Gibson [26]. Gibson's equations are essentially shallow shell equations, but the shallow shell approximations are not used consistently when particular loadings are considered. That is, exact trigonometric representations for the tangential and normal loads are employed, and the solution integrals are evaluated over the actual shell surface rather than over the base plane. These factors have an appreciable effect in the present problem because the shell is only marginally shallow. Hence, in order for the finite element results to be comparable with these exact results, the same procedures must be introduced here. This is easily done by expanding the trigonometric load variations up to second order within each element by Taylor's

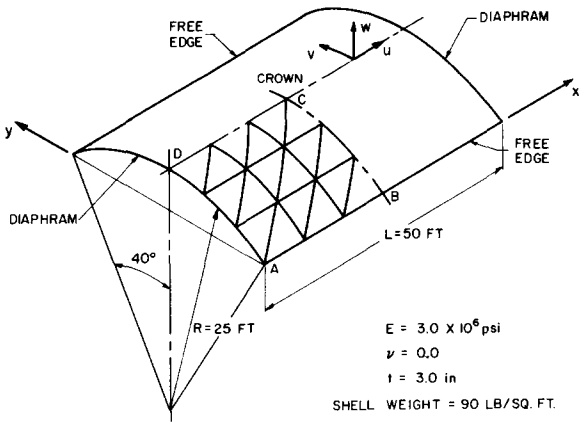

FIG. 11. Cylindrical shell roof configuration (3 × 3 grid shown).

series. The consistent load matrices are then obtained in closed form following the procedure of Section 2.4. Further, the area of integration for both the stiffness and load matrices is taken equal to that of the actual shell surface. Finally, it is noted that Gibson's symmetric series solution was carefully programmed, and accurate calculations were obtained for the quantities of interest. These exact calculations differ somewhat from those given by Carr [5], but no explanation for these discrepancies has been found.

Some of the most pertinent numerical results are given in Table 6 and convergence plots for these quantities are given in Fig. 12. It is seen again that the approximations obtained with even the coarsest gridworks are exceedingly accurate, and the convergence is again very rapid. In particular, the slopes of the error curves for displacements and strain energy are all about -5.

TABLE 6. NUMERICAL RESULTS FOR CYLINDRICAL SHELL ROOF PROBLEM

Finite element grids	$10u_A$ (in.)	w_B (in.)	$10v_B$ (in.)	$10w_C$ (in.)
1 × 1	−0·9158	−1·21672	−3·96349	0·2228
2 × 2	−1·3954	−3·66312	−8·08975	4·5518
3 × 3	−1·49497	−4·03037	−8·65809	5·1446
4 × 4	−1·51050	−4·08388	−8·73995	5·2258
Exact	−1·51325	−4·09916	−8·76147	5·2494

$10^{-3}N_{xxB}$ (lb./in.)	$10^{-3}M_{yyC}$ (lb. in./in.)	$10^{-2}M_{xxC}$ (lb. in./in.)	10^{-4} × strain energy (lb./in.)
5·3637	1·5437	2·994	2·78548
6·9845	2·3463	4·498	5·37577
6·6313	2·1571	2·127	5·79980
6·5016	2·0871	1·284	5·86511
6·4124	2·0562	0·9272	5·88277

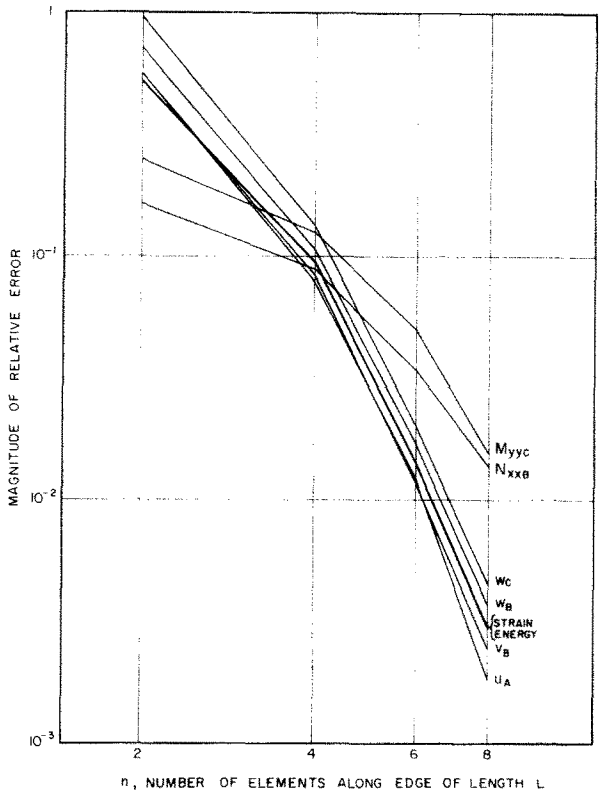

FIG. 12. Relative error of finite element solutions for cylindrical shell roof problem.

The quantity which has been used by many authors for comparison purposes is the vertical deflection of point B (Fig. 11). Such a comparison is given in Fig. 13 where the abscissa is the total number of degrees of freedom (before boundary conditions) required with the various finite element representations. It is clear that this comparison favours the present results in that it shows that the present element yields the best accuracy for the minimum number of degrees of freedom. It is interesting to note that the results of Refs. [5] and [13] have not actually converged to the exact solution even though more than 1000 degrees of freedom were used.

4. CONCLUSIONS

A conforming shallow shell element of arbitrary triangular shape has been presented. The element may be used to solve shallow shell problems with a wide variety of boundary shapes. The examples presented demonstrate that the element provides excellent accuracy and rapid convergence. In fact, the theoretical asymptotic rate of convergence of strain energy is n^{-6}. Unique values of stresses are obtained directly at nodal points. Accurate predictions of membrane force and bending moment distributions, as well as displacement distributions were obtained in all the examples using only a few elements.

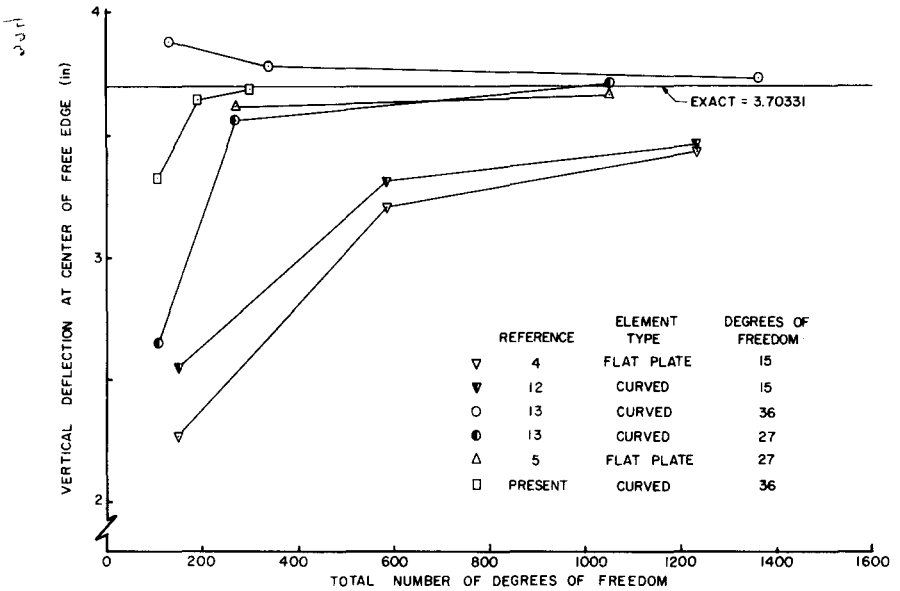

FIG. 13. Cylindrical shell roof problem comparisons.

The present work represents the first step in extending the successful approach used in the high precision triangular plate bending element to shells. The next step will involve a general deep shell formulation.

REFERENCES

[1] R. E. JONES and D. R. STROME, A survey of analysis of shells by the displacement method. *Matrix Methods in Structural Mechanics*. Wright-Patterson AFB, AFFDL-TR-80 (1966).

[2] A. HRENNIKOFF and S. S. TEZCAN, Analysis of cylindrical shells by the finite element method. *Symp. on Problems of Interdependence of Design and Construction of Large-Span Shells for Industrial and Civic Buildings*. Leningrad (1966).

[3] O. C. ZIENKIEWICZ and Y. K. CHEUNG, *The Finite Element Method in Structural and Continuum Mechanics*. McGraw-Hill (1967).

[4] R. W. CLOUGH AND R. J. JOHNSON, A finite element approximation for the analysis of thin shells. *Int. J. Solids Struct.* **4**, 43–60 (1968).

[5] A. J. CARR, A refined finite element analysis of thin shell structures including dynamic loadings. Ph.D. Thesis, University of California, Berkeley (1967).

[6] F. K. BOGNER, R. L. FOX and L. A. SCHMIT, A cylindrical shell discrete element. *AIAA Jnl* **5**, 745–750 (1967).

[7] G. CANTIN and R. W. CLOUGH, A curved, cylindrical shell, finite element. *AIAA Jnl* **6**, 1057–1062 (1968).

[8] M. D. OLSON and G. M. LINDBERG, Vibration analysis of cantilevered curved plates using a new cylindrical shell finite element. *Proc. 2nd Conf. on Matrix Methods in Structural Mechanics*. Wright-Patterson AFB, Ohio (1968).

[9] J. J. CONNOR and C. BREBBIA, Stiffness matrix for shallow rectangular shell element. *J Engng Mech. Div., Amer. Soc. civ. Engrs* **93**, EM5, 43–65 (1967).

[10] R. H. GALLAGHER, The development and evaluation of matrix methods of thin shell structural analysis. Ph.D. Thesis, State University of New York (1966).

[11] S. UTKU and R. J. MELOSH, Behavior of triangular shell element stiffness matrices associated with polyhedral deflection distributions. AIAA Paper No. 67-114, AIAA Sixth Aerospace Sciences Meeting, New York (1967). [Also *AIAA Jnl* **6**, 374–376 (1968).]

[12] G. E. STRICKLAND and W. A. LODEN, A doubly-curved triangular shell element. *Proc. 2nd Conf. on Matrix Methods in Structural Mechanics*. Wright-Patterson AFB, Ohio (1968).

[13] G. BONNES, G. DHATT, Y. M. GIROUX and L. P. A. ROBICHAUD, Curved triangular elements for the analysis of shells. *Proc. 2nd Conf. on Matrix Methods in Structural Mechanics*. Wright-Patterson AFB, Ohio (1968).
[14] G. R. COWPER, E. KOSKO, G. M. LINDBERG and M. D. OLSON, Formulation of a new triangular plate bending element. *Can. Aero. Space Inst. Trans.* **1**, 86–90 (1968).
[15] G. R. COWPER, E. KOSKO, G. M. LINDBERG and M. D. OLSON, A high precision triangular plate bending element. National Research Council of Canada Aero. Report LR-514 (1968).
[16] G. R. COWPER, E. KOSKO, G. M. LINDBERG and M. D. OLSON, Static and dynamic applications of a high precision triangular plate bending element. *AIAA Jnl* **7**, 1957–1965 (1969).
[17] K. BELL, *Analysis of Thin Plates in Bending Using Triangular Finite Elements*. Institutt for Statikk, Norges Tekniske Hogskole, Trondheim, Norway (1968).
[18] K. BELL, A refined triangular plate bending finite element. *J. Numer. Meth. Engng* **1**, 101–120 (1969).
[19] G. A. BUTLIN and R. FORD, A compatible triangular plate bending finite element. University of Leicester, Eng. Dept. Report 68-15 (1968).
[20] C. A. FELIPPA, Refined finite element analysis of linear and nonlinear two-dimensional structures. Ph.D. Thesis, University of California, Berkeley (1966).
[21] V. V. NOVOZHILOV, *The Theory of Thin Shells*, 2nd Edition, Section 17a. Noordhoff (1964).
[22] S. TIMOSHENKO and J. N. GOODIER, *Theory of Elasticity*, 2nd Edition, Section 51. McGraw-Hill (1951).
[23] S. TIMOSHENKO and S. WOINOWSKY-KRIEGER, *Theory of Plates and Shells*, 2nd Edition, Section 44. McGraw-Hill (1959).
[24] S. A. AMBARTSUMYAN, On the calculation of shallow shells. NACA TM 1425 (1956).
[25] A. C. SCORDELIS and K. S. LO, Computer analysis of cylindrical shells. *J. Am. Concr. Inst.* **61**, 539–561 (1964).
[26] J. E. GIBSON, *The Design of Cylindrical Shell Roofs*, 2nd Edition. E. & F. N. Spon (1961).

APPENDIX

Conformity requirements

A finite element is said to be conforming if the displacements have sufficient inter-element continuity to satisfy the admissibility requirements of the theorem of minimum potential energy. For shells, the appropriate continuity requirements are that the displacement vector and the edgewise component of the rotation vector are continuous between elements. In discussing conformity requirements for shallow shells it is helpful to distinguish two cases: (a) smooth shells in which the slopes ζ_x, ζ_y, are continuous everywhere, and (b) shells with kinks, i.e. shells in which discontinuities in ζ_x, ζ_y, occur.

In the case of smooth shells, continuity of displacement requires that the individual components u, v, w, be continuous. Continuity of edgewise rotation is assured if the derivatives w_x, w_y are continuous. The situation here may be contrasted with the situation in deep shells. For deep shells the rotations are given by expressions of the form $w_x + u/R$ where R is a radius of curvature. In shallow shells the terms u/R are neglected, so that conformity requires only that w_x, w_y, be continuous. Furthermore, discontinuities in the radii of curvature have no influence on the conformity requirements for shallow shells. These conclusions can be verified by considering the variation of the strain energy of an element. From equation (4), this variation may be calculated as

$$\begin{aligned}\delta U &= \int\int \{N_{\xi\xi}\delta\varepsilon_{\xi\xi} + N_{\eta\eta}\delta\varepsilon_{\eta\eta} + N_{\xi\eta}\delta\varepsilon_{\xi\eta} + M_{\xi\xi}\delta\kappa_{\xi\xi} + M_{\eta\eta}\delta\kappa_{\eta\eta} + M_{\xi\eta}\delta\kappa_{\xi\eta}\}\,\mathrm{d}\xi\,\mathrm{d}\eta \\ &= \int\int \{N_{\xi\xi}(\delta u_\xi - \zeta_{\xi\xi}\delta w) + N_{\eta\eta}(\delta v_\eta - \zeta_{\eta\eta}\delta w) + N_{\xi\eta}(\delta u_\eta + \delta v_\xi - 2\zeta_{\xi\eta}\delta w) \\ &\qquad - M_{\xi\xi}\delta w_{\xi\xi} - M_{\eta\eta}\delta w_{\eta\eta} - 2M_{\xi\eta}\delta w_{\xi\eta}\}\,\mathrm{d}\xi\,\mathrm{d}\eta \qquad (29)\end{aligned}$$

where $M_{\xi\xi}$, $N_{\xi\xi}$, etc., are the stress resultants and bending moments given by

$$N_{\xi\xi} = C(\varepsilon_{\xi\xi} + \nu\varepsilon_{\eta\eta}) \qquad N_{\eta\eta} = C(\varepsilon_{\eta\eta} + \nu\varepsilon_{\xi\xi}) \qquad N_{\xi\eta} = C(1-\nu)\varepsilon_{\xi\eta}/2$$
$$M_{\xi\xi} = D(\kappa_{\xi\xi} + \nu\kappa_{\eta\eta}). \qquad M_{\eta\eta} = D(\kappa_{\eta\eta} + \nu\kappa_{\xi\xi}) \qquad M_{\xi\eta} = D(1-\nu)\kappa_{\xi\eta}/2$$

with $C = Et/(1-\nu^2)$. By integration by parts and use of the divergence theorem, the integral in (29) can be transformed to

$$\begin{aligned}\delta U = \oint \{&(\delta u N_{\xi\xi} + \delta v N_{\xi\eta} + \delta w Q_\xi - \delta w_\xi M_{\xi\xi} - \delta w_\eta M_{\xi\eta})\,\mathrm{d}\eta \\ &-(\delta u N_{\xi\eta} + \delta v N_{\eta\eta} + \delta w Q_\eta - \delta w_\xi M_{\xi\eta} - \delta w_\eta M_{\eta\eta})\,\mathrm{d}\xi\} \\ &-\int\int \left\{\delta u\left(\frac{\partial N_{\xi\xi}}{\partial\xi} + \frac{\partial N_{\xi\eta}}{\partial\eta}\right) + \delta v\left(\frac{\partial N_{\xi\eta}}{\partial\xi} + \frac{\partial N_{\eta\eta}}{\partial\eta}\right)\right. \\ &+\delta w\left(\frac{\partial Q_\xi}{\partial\xi} + \frac{\partial Q_\eta}{\partial\eta} + \zeta_{\xi\xi}N_{\xi\xi} + 2\zeta_{\xi\eta}N_{\xi\eta} + \zeta_{\eta\eta}N_{\eta\eta}\right) \\ &\left.-\delta w_\xi\left(\frac{\partial M_{\xi\xi}}{\partial\xi} + \frac{\partial M_{\xi\eta}}{\partial\eta} - Q_\xi\right) - \delta w_\eta\left(\frac{\partial M_{\xi\eta}}{\partial\xi} + \frac{\partial M_{\eta\eta}}{\partial\eta} - Q_\eta\right)\right\}\,\mathrm{d}\xi\,\mathrm{d}\eta \end{aligned} \tag{30}$$

where Q_ξ, Q_η, are the usual transverse shearing forces. In view of the equilibrium equations for shallow shells, the surface integral in (30) reduces to the expression for the virtual work of the applied loads. Thus,

$$\begin{aligned}\delta U = \oint \{&(\delta u N_{\xi\xi} + \delta v N_{\xi\eta} + \delta w Q_\xi - \delta w_\xi M_{\xi\xi} - \delta w_\eta M_{\xi\eta})\,\mathrm{d}\eta \\ &-(\delta u N_{\xi\eta} + \delta v N_{\eta\eta} + \delta w Q_\eta - \delta w_\xi M_{\xi\eta} - \delta w_\eta M_{\eta\eta})\,\mathrm{d}\xi\} \\ &+\int\int (Q_u\delta u + Q_v\delta v + Q_w\delta w)\,\mathrm{d}\xi\,\mathrm{d}\eta. \end{aligned} \tag{31}$$

The conformity requirements may be deduced from the contour integral in (31), since inter-element continuity of the integrands therein is essential for the validity of the theorem of minimum potential energy. It is seen that it is sufficient for u, v, w and the first derivatives of w to be continuous, and hence the element presented in this paper is fully conforming for smooth shells.

The situation, however, is different in non-smooth shells. If a kink occurs along an inter-element boundary the normal to the shell surface is discontinuous between elements. The continuity of the displacement vector then is no longer a simple matter of continuity of the individual components. Instead, continuity involves linear relations between individual components. In this case then, strict continuity cannot be obtained with the present element because of the difference in degree between the polynomial used for w and the polynomials used for u and v.

(*Received* 28 *April* 1969; *revised* 23 *October* 1969)

Абстракт—Обсуждается конечный элемент соответствующей пологой оболочки, произвольной трехугольной формы, который принимается для решения некоторых статических задач. Этот элемент содержит 36 обобщенных координат, именно: нормальное перемещение w и его первые и вторые производные плюс тангенциальные перемещения u и v и их первые производные при каждой вершине. Используя этот элемент, теоретическая асимптотическая скорость сходимости энергии деформации равняется n^{-6}, где n–число элементов на некоторой части структуры. Представленные применения указывают, что, в данном случае, получается правильное определение так напряжений как и перемещений с помощью незначительного числа элементов.